Dimension reduction of homoclinic orbits of buckled beams via the nonlinear normal modes technique

Stefano Lenci, Giuseppe Rega

Author's Accepted Manuscript

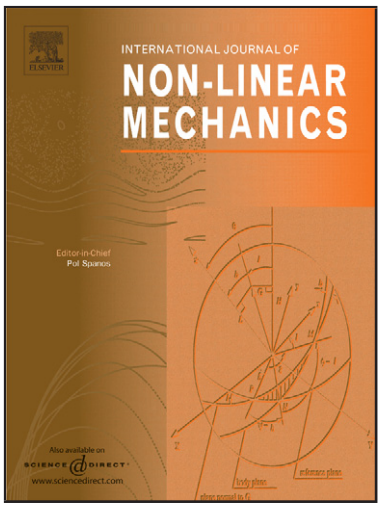

www.elsevier.com/locate/nlm

Dimension reduction of homoclinic orbits of buckled beams via the nonlinear normal modes technique

Stefano Lenci, Giuseppe Rega

PII: S0020-7462(07)00057-1
DOI: doi:10.1016/j.ijnonlinmec.2007.02.004
Reference: NLM 1342

To appear in: *International Journal of Non-Linear Mechanics*

Received date: 22 August 2006
Revised date: 28 December 2006
Accepted date: 13 February 2007

Cite this article as: Stefano Lenci and Giuseppe Rega, Dimension reduction of homoclinic orbits of buckled beams via the nonlinear normal modes technique, *International Journal of Non-Linear Mechanics* (2007), doi:10.1016/j.ijnonlinmec.2007.02.004

Dimension reduction of homoclinic orbits of buckled beams via the nonlinear normal modes technique

STEFANO LENCI

Dipartimento di Architettura, Costruzioni e Strutture, Università Politecnica delle Marche via Brecce Bianche, 60131, Ancona, Italy, Lenci@univpm.it

GIUSEPPE REGA

Dipartimento di Ingegneria Strutturale e Geotecnica, Università di Roma "La Sapienza" via A. Gramsci 53, 00197, Roma, Italy, Giuseppe.Rega@uniroma1.it

Abstract. The problem of detecting the homoclinic orbits of an initially straight buckled beam is addressed. Two families of b.c. are identified and investigated in detail. For the first family, the homoclinic orbits belong to a planar invariant manifold, and are easily computed in closed form. For the second family, the manifold is no longer planar, and is detected via the nonlinear normal modes technique by obtaining approximate expressions which are sufficient to highlight the effects of the non-flatness. A hierarchy of reduced order, single degree of freedom, models is determined. These are obtained by taking into account increasing degrees of nonlinearity in the potential energy, which allow for a more and more refined computation of the homoclinic solution. The various models are compared with each other and discussed in detail, and the non-planarity of the manifold is illustrated through examples.

Keywords: Buckled beam; infinite dimensional system; homoclinic solutions; higher-order modes; reduced order models; nonlinear normal modes.

1. Introduction

All people working on nonlinear dynamics and chaos of engineering systems become aware of the importance of homoclinic orbits, sooner or later. These are particular solutions of the governing equations connecting, in an infinite time, a given unstable equilibrium point. In spite of the fact that they are special and isolated solutions, they play a fundamental role in the organization of the *global* dynamics of complex systems, as repeatedly verified in practice (e.g., [1-3]). They also play a fundamental role in the study of spatial chaos [4].

In the past, these solutions have been studied on systems with few (usually one) mechanical degrees of freedom (d.o.f.), which are governed by ordinary differential equations (ODEs) [5]. However, real mechanical structures are infinite dimensional, namely they are governed by partial differential equations (PDEs), and call for a more refined analysis.

The study of the homoclinic solutions in infinite dimensional systems is the main objective of

this paper, where it is addressed with reference to an initially straight, planar, undamped and unforced buckled beam. While in low dimensional systems the homoclinic solutions can usually be computed, so that their existence is guaranteed, in infinite dimension their existence is initially conjectured based on system mechanical properties. In this respect, the results of this paper could be used, at least in principle, to prove *a posteriori* that the homoclinic solutions actually exist, would one be able to compute all terms of the series used for their representation, and to prove its convergence. We will not address this issue in this mechanically oriented paper, being satisfied of the mechanical conjecture about their existence. For the same reason, only few terms of the mentioned series will be computed, by discussing how they can be sufficient for practical purposes.

We focus on the *analytical* detection of homoclinic orbits, which is possible because we consider the hilltop saddle of a conservative system. More general cases have to be dealt with numerically, even for low dimensional ODEs [6]. Yet, we believe that the case considered in this work, which aims at enlightening how to address large dimensionality and obtaining information about its main effects, can help also in view of a purely numerical approach.

The main source of difficulty is that the homoclinic solutions are expected to activate all spatial linear normal modes of the beam, thus entailing a full nonlinear modal coupling. We assume that the homoclinic orbits belong to a *two dimensional invariant* manifold, which is *not* expected to be *planar* in the space spanned by the linear modes. Such a manifold is the set where the dynamics we are interested in lie. Its existence is conjectured based on similar results holding for finite dimensional systems [5], and again it would be proved *a posteriori* should one succeed in showing the convergence of the series used for its detection. In turn, if the manifold is two dimensional, the dynamics embedded on it are governed by two mathematical d.o.f., corresponding to a single mechanical d.o.f.. This suggests a 'structure' to occur in the associated homoclinic solutions, which can be described by a *proper* reduced order model, possibly different from those obtained with classical dimensional reduction techniques, such as the linear Galerkin method. Thus, we naturally fall in the realm of dimension reduction, which is a matter of intensive on-going research (see, e.g., [7-9]) aimed at improving the accuracy of the reduced models.

Among various competing approaches, in this paper we use the nonlinear normal modes techniques to detect the manifold, the homoclinic orbits and the reduced order model lurking in the background, thus obtaining all information of interest within a comprehensive investigation. We closely follow the approach of [10], which is similar to the center manifold reduction [11], and permits the detection of searched quantities in either exact or approximate ways. In fact, the results will be given in terms of a series, and one can consider only few terms for practical purposes. Of course, the number of required terms depends on the searched accuracy.

An appealing viewpoint on the nonlinear normal modes (NNMs) of continuous systems, which somehow enlightens the relevant nature, consists in regarding them as mathematical structures accounting for *time change* of the system *spatial* shape, which instead remains fixed in linear oscillations if initially corresponding to a linear normal mode.

The idea of NNMs was introduced by Rosenberg [12], and later theoretical and practical important contributions were given by Rand [13] and by Vakakis [14]. Shaw and Pierre [15-16] were the first to consider the NNMs as an invariant manifold tangent to the space spanned by the linear modes in phase space, which is the viewpoint followed in this paper. When applied to infinite-dimensional systems, this approach requires a previous projection of the dynamics onto the linear normal modes, so that the PDE of motion is transformed into a sequence of coupled nonlinear ODEs, which is the natural framework for the geometric approach to NNMs. Then, the machinery of invariant manifolds applies [17].

A different approach to NNMs, not pursued in this work, has also been proposed [18-19] and investigated at length. It is based on directly attacking the PDE via an asymptotic development method, with no *a priori* projection of the solution onto linear normal modes. The coupling among modes ensues *a posteriori* from the infinite-dimensional analysis.

NNMs were originally developed to deal with classical nonlinear oscillations, and synthesize the effects of the nonlinearity. In this context they have been investigated in depth and developed along various research paths, with reference to various mechanical and structural systems, which include shallow arches and cables [20-21], single beams [17], frames [22], rotor blades [23] and MEMS [24]. In this paper, they are used to detect homoclinic orbits. The authors are not aware of previous works in this direction.

The paper is organized as follows. In Sect. 2 the mechanical model and the associated partial differential equation are set, paying attention to distinguish between two families of boundary conditions giving different behaviour in terms of homoclinic solutions. The linear modal analysis is performed in Sect 3, where the projected nonlinear equations are also obtained. The nonlinear normal modes are considered in Sect. 4, where the invariant manifold containing the homoclinic orbits is determined by solving the appropriate modal equations. The dynamics on the manifold, and the homoclinic solutions, are studied in Sect. 5, where a hierarchy of approximate reduced order models is established. The paper ends (Sect. 6) with some conclusions and suggestions for further developments.

2. The mechanical model

The dimensionless partial differential equation governing the unforced undamped planar nonlinear dynamics of an initially straight buckled beam is

$$\ddot{w}+w''''+\Gamma w''-kw''\int_0^1 (w')^2\,dz=0, \tag{1}$$

where $w(z,t)$ is the time dependent transversal displacement of the point at abscissa $z\in[0,1]$, dot and prime represent derivatives with respect to time and space, respectively, and k is the stiffness due to membrane effects. The parameter $\Gamma>\Gamma_{cr}$ represents the first-order axial load (positive=compression, Γ_{cr}=buckling critical parameter) associated with a finite prescribed end-displacement of the beam in the axial direction [25-26].

Equation (1) describes the finite amplitude transverse dynamics of the buckled beam under the classical Kirchhoff assumption [27] of neglecting the longitudinal inertia, also known in the literature as statically condensed model. It permits feasible computations and analytical developments without losing the main mechanical phenomena, at least for moderate displacements, which are implicitly assumed without further remarks. System (1) is conservative, with the Hamilton and potential functions being, respectively

$$H(\dot{w},w)=\frac{1}{2}\left(\int_0^1 \dot{w}^2 dz\right)+V(w),\qquad V(w)=-\frac{\Gamma}{2}\left(\int_0^1 w'^2\,dz\right)+\frac{1}{2}\left(\int_0^1 w''^2\,dz\right)+\frac{k}{4}\left(\int_0^1 w'^2\,dz\right)^2. \tag{2}$$

When $\Gamma>\Gamma_{cr}$ and irrespective of the type of transverse boundary conditions, the undeformed equilibrium position of system (1) (which now is a hilltop saddle point) has one stable and one unstable direction, and we assume that they are connected by an homoclinic orbit. As the mechanical system is symmetric, namely, if $w(z,t)$ is a solution also $-w(z,t)$ is a solution, the homoclinic orbits are always in couple.

2.1. Boundary conditions

To make the problem (1) well-posed, initial and boundary conditions must be added. While initial conditions are not important, as we consider global system dynamics and not specific trajectories, boundary conditions (b.c.) play a significant role in successive developments. If the constraints are supposed to be not elastic, we can assume on each boundary one condition between $w=0$ and $w'''+\Gamma w'=0$, and another condition between $w''=0$ and $w'=0$. Excluding repetitions and kinematically not admissible b.c., the six basically different b.c. are reported in Table 1, where they are grouped in two different families.

Looking for an *exact* solution of nonlinear equation (1) in the form $w(z,t)=a(t)b(z)$ requires $b''''\propto b''\propto b$, namely, $b''=\kappa b$ for an arbitrary κ. If κ is positive, this equation has solution $b(z)=c_1\sinh(z\sqrt{\kappa})+c_2\cosh(z\sqrt{\kappa})$, while for κ negative the solution is $b(z)=c_1\sin(z\sqrt{(-\kappa)})+c_2\cos(z\sqrt{(-\kappa)})$. As we have only the two unknowns c_1 and c_2, in general there is no hope to satisfy all four b.c.

associated to (1). This occurs only for the two special cases of Table 1, which constitute the first family. For the hinged-hinged beam (Fig. 1a) we have $b(z)=w_n(z)=\sqrt{2}\sin(n\pi z)$, $n=1,2,3,\ldots$, while for the guided-hinged beam (Fig. 1b) we have $b(z)=w_n(z)=\sqrt{2}\cos[(n\pi-\pi/2)z]$, $n=1,2,3,\ldots$.

In both cases we have $w_n=0$ or $w_n'=0$ at the boundary, and

$$\int_0^1 w_n' w_m' dz = -\kappa_n \delta_{nm}, \tag{3}$$

where $\kappa_n=-(n\pi)^2$ for the hinged-hinged beam, and $\kappa_n=-(n\pi-\pi/2)^2$ for the guided-hinged beam, δ_{nm} being the Kronecker delta. This is a very important orthogonality property of this family of b.c., which will be properly exploited in the following.

$z=0$					$z=1$					
w	$w'''+\Gamma w'$	w'	w''	*name*	w	$w'''+\Gamma w'$	w'	w''	*name*	
x			x	hinged	x			x	hinged	first family
x			x	hinged		x	x		guided	first family
x		x		fixed	x		x		fixed	second family
x		x		fixed	x			x	hinged	second family
x		x		fixed		x	x		guided	second family
x		x		fixed		x		x	free	second family

Table 1. The boundary conditions of the first and of the second family.

The b.c. not fulfilling the previous requirement belong to the second family (Fig. 2), for which no exact solution in separate variables form does exist: They are the fixed-fixed (a), the fixed-hinged (b), the fixed-free (c) and the fixed-guided (d) beams.

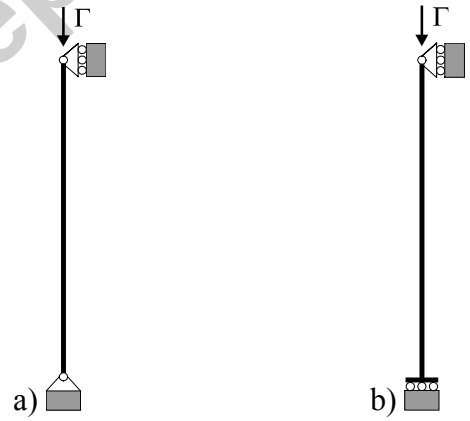

Figure 1. The first family of b.c.: a) hinged-hinged and b) guided-hinged.

The previous distinction has not only a mathematical character, but also an important dynamical meaning. In fact, we will see that for the first class of b.c. the invariant manifold Σ on which the

homoclinic loop (which is the principal part of the dynamics herein considered) lies is flat, while in the other case it is non planar (Sect. 4).

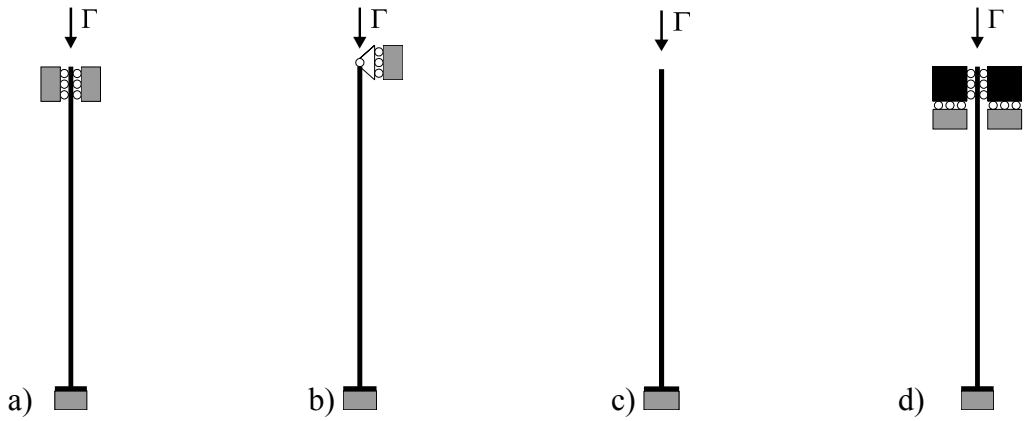

Figure 2. The second family of b.c.: a) fixed-fixed, b) fixed-hinged, c) fixed-free and d) fixed-guided.

3. Linear normal modes and projected nonlinear equations of motion

The spatial linear operator appearing in (1) is $L(w)=w''''+\Gamma w''$, and their eigenvalues $\Lambda_n(\Gamma)$ and eigenfunctions $w_n(z;\Gamma)$ satisfy the equation $w_n''''+\Gamma w_n''=\Lambda_n w_n$, whose general solution can be written in the form

$$w_n(z)=c_1\cos(\alpha z)+c_2\sin(\alpha z)+c_3\cosh(\beta z)+c_4\sinh(\beta z),$$

$$\alpha=\sqrt{\frac{\Gamma+\sqrt{\Gamma^2+4\Lambda_n}}{2}},\ \beta=\sqrt{\frac{-\Gamma+\sqrt{\Gamma^2+4\Lambda_n}}{2}}\,. \tag{4}$$

The eigenvalues Λ_n are determined by the boundary conditions. The mathematical properties of $L(w)$ (basically because it is self-adjoint for all b.c.) guarantee that they are real, that

$$\int_0^1 w_n w_m dz=\delta_{nm},\qquad \int_0^1 w_n'' w_m'' dz-\Gamma\int_0^1 w_n' w_m' dz=\Lambda_n\delta_{nm}, \tag{5}$$

and that the eigenfunctions constitute a basis of the displacement field, so that the solution can be sought in the form

$$w(z,t)=\sum_{n=1}^{\infty} a_n(t)w_n(z)\,. \tag{6}$$

The eigenfunctions are called linear normal modes. They span a planar invariant (with respect to the linearized equations) manifold in the space of admissible functions.

For the hinged-hinged and guided-hinged beams we have, respectively, the expressions

$$\Lambda_n=(n\pi)^2[(n\pi)^2-\Gamma], \qquad w_n(z)=\sqrt{2}\,\sin(n\pi z), \tag{7}$$

$$\Lambda_n=(n\pi-\pi/2)^2[(n\pi-\pi/2)^2-\Gamma], \qquad w_n(z)=\sqrt{2}\,\cos[(n\pi-\pi/2)z], \tag{8}$$

which are somehow special because the two cases belong to the first family of b.c., as they satisfy $w_n''=\kappa_n w_n$. The relevant eigenvalues are linear functions of Γ.

For the second family, the expressions of the eigenvalues and eigenfunctions are more involved, and are better illustrated by means of the diagrams in Fig. 3.

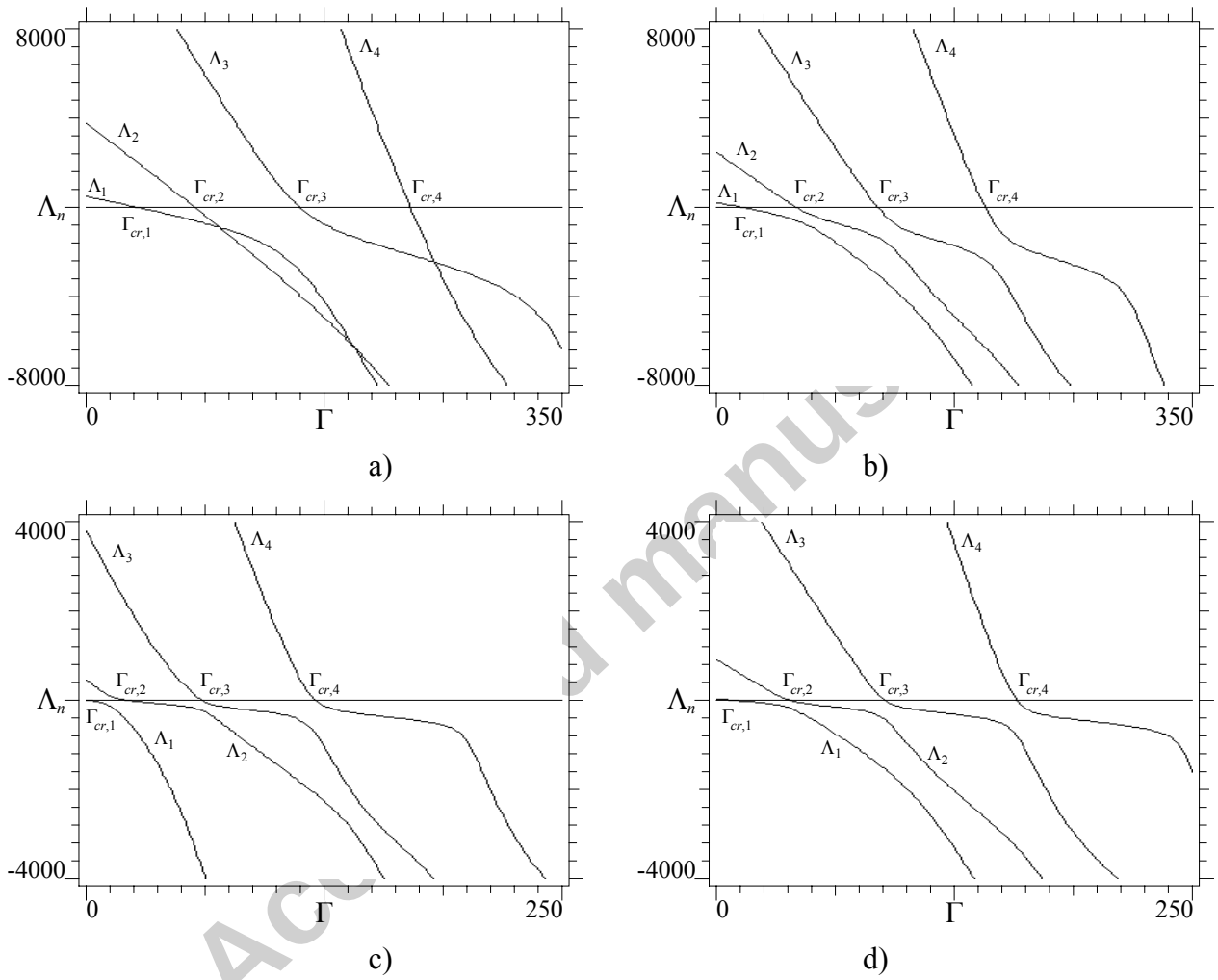

Figure 3. The first four eigenvalues for a) fixed-fixed, b) fixed-hinged, c) fixed-free and d) fixed-guided beams.

The eigenvalues are decreasing functions of the axial parameter Γ. The unique value $\Gamma_{cr,n}$ where they vanish is the n-th buckling parameter. Positive and negative values of Λ_n correspond to stable and unstable linear normal mode, respectively. In the former case, $\sqrt{\Lambda_n}$ is the n-th natural frequency. The homoclinic orbits we are interested in may exist only when the beam is buckled, i.e., for $\Gamma>\Gamma_{cr,1}$ and $\Lambda_1<0$, otherwise there would be no unstable direction of the hilltop saddle.

Consequently, we make this assumption in the following.

Inserting the expression (6) in (2), and using the properties (5) we get

$$H(\dot{a}_n, a_n)=\frac{1}{2}\sum_{n=1}^{\infty}(\dot{a}_n)^2+V(a_n), \qquad V(a_n)=\frac{1}{2}\sum_{n=1}^{\infty}\Lambda_n(a_n)^2+\frac{k}{4}\left(\sum_{n=1}^{\infty}\sum_{m=1}^{\infty}a_n a_m d_{n,m}\right)^2,$$

$$d_{m,n}=d_{n,m}=\int_0^1 w_n' w_m' dz\,, \tag{9}$$

from which the governing equations easily follow:

$$\ddot{a}_n+\frac{\partial V}{\partial a_n}=\ddot{a}_n+\Lambda_n a_n+k\left(\sum_{i=1}^{\infty}\sum_{j=1}^{\infty}a_i a_j d_{i,j}\right)\left(\sum_{m=1}^{\infty}a_m d_{n,m}\right)=0. \tag{10}$$

It is worth to note that the nonlinear coefficients $d_{n,m}$ depend on only the axial parameter Γ.

For the first family of b.c. we have $d_{n,m}=-\kappa_n\delta_{nm}$ (see eq. (3)), so that the equations of motion become

$$\ddot{a}_n+\Lambda_n a_n+k\kappa_n a_n\left(\sum_{i=1}^{\infty}\kappa_i a_i^2\right)=0, \tag{11}$$

which exhibit only the minor coupling given by the single summation. From (11) we see that if we start with an initial condition such that $a_n\neq 0$, $\dot{a}_n\neq 0$, for a given n, and $a_i=\dot{a}_i=0$, $i\neq n$, then a_i and $\dot{a}_i$, $i\neq n$, remain null for all time, while the time evolution of a_n is governed by the hardening Duffing equation

$$\ddot{a}_n+\Lambda_n a_n+k\kappa_n^2 a_n^3=0. \tag{12}$$

In dynamical systems language [5], this means that the eigenspaces spanned by the linear modes, which are planar in the linearized case, remain planar also in the nonlinear one, or, equivalently, that the NNMs coincide with the linear ones. For the b.c. of the second family, on the other hand, we have a full nonlinear coupling among modes, and the invariant manifolds no longer remain planar when nonlinearities are considered.

4. Invariant manifold and homoclinic solutions (nonlinear normal modes technique)

The homoclinic solutions are special cases of the expression (6), $w_{\text{hom}}(z,t)=\sum_{n=1}^{\infty}a_{n,\text{hom}}(t)w_n(z)$, whose time-dependent amplitudes $a_{n,\text{hom}}(t)$ correspond to vanishing of the Hamiltonian $(9)_1$. Many

homoclinic solutions of the hilltop saddle can exist in principle, corresponding to stable and unstable directions of different order. However, we focus attention on only the principal one, namely on the homoclinic solution related to the lowest order, stable and unstable, directions. As we conjectured in the Introduction, they belong to a two dimensional invariant (with respect to the nonlinear equations) manifold Σ which in general is not planar and is difficult to be handled. To overcome this point, the NNM technique, which also allows us to obtain reliable reduced order models, is used [16, 28-29]. Although it was originally developed to deal with nonlinear oscillations, herein it is applied to homoclinic orbits.

Three issues are addressed in this section. (i) The presentation of the master-slave technique used to detect the invariant manifold, which includes obtaining the slave equations, (ii) its specification for the homoclinic orbits, and (iii) its application to the two families of b.c. As a matter of fact, the first family can be dealt with without resorting to the NNM technique, so that this section is really needed for only the second family.

Following the treatment of [10] (see also the introductory paper in [9] for an overall framework), we identify a main, or *master*, variable (i.e., modal amplitude) x and consider the others as secondary, or *slave*, variables. Because in the buckled beam problem the unstable direction triggering the homoclinic orbit we are looking for is wherever along the first eigenfunction, apart from the range in Fig. 3a where $\Lambda_2<\Lambda_1$, it is natural to assume $x=a_1$, while a_i, $i\geq 2$, namely the higher order modal amplitudes, are the slave variables. Note that around the crossover points of Fig. 3a we need two master variables for a consistent analysis, but this is out of the scope of the present work.

The key idea of the method consists in assuming that the slave variables can be expressed as *time-independent* functions of the master one:

$$a_i=a_i(x), \quad i\geq 2. \tag{13}$$

If we use only N terms in (6) this relation provides an approximation of the searched manifold Σ (approximate manifold), while for $N\to\infty$ it exactly gives Σ (exact manifold).

Differentiating (13) with respect to time we get, by the chain rule,

$$\dot{a}_i=\frac{da_i}{dt}=\frac{da_i}{dx}\frac{dx}{dt}=a_i'\,\dot{x}, \qquad \ddot{a}_i=a_i''\,\dot{x}^2+a_i'\,\ddot{x}, \qquad i\geq 2. \tag{14}$$

Combining $(14)_2$ with (10) yields

$$\frac{\partial V}{\partial a_i}=-a_i''\,\dot{x}^2+a_i'\frac{\partial V}{\partial x}, \qquad i\geq 2, \tag{15}$$

while $(9)_1$ and $(14)_1$ give

$$2[H(x,a_i)-V(x,a_i)]=\dot{x}^2[1+\sum_{j=2}^{\infty}(a_j')^2]. \tag{16}$$

Eliminating $\dot{x}^2$ from (15) and (16), we obtain

$$2[V-H]a_i''+[1+\sum_{j=2}^{\infty}(a_j')^2]\left(a_i'\frac{\partial V}{\partial x}-\frac{\partial V}{\partial a_i}\right)=0, \quad i\geq 2, \tag{17}$$

which are the *slave equations* (corresponding to the *modal equations* in Rand [10]).

To apply the previous general theory to *homoclinic* orbits we note that on these solutions it is $H=0$, so that the strongly nonlinear ODEs permitting to determine the unknown functions (13) read:

$$2Va_i''+[1+\sum_{j=2}^{\infty}(a_j')^2]\left(a_i'\frac{\partial V}{\partial x}-\frac{\partial V}{\partial a_i}\right)=0, \quad i\geq 2, \tag{18}$$

where we have still written a_i instead of $a_{i,\mathrm{hom}}$, for the sake of simplicity. Actually, they are much more complex than the original system (10), and their introduction may appear useless. Nonetheless, they contain only polynomial terms and, since we are interested in the finite – though non necessarily small – neighborhood of $x=0$ where the homoclinic solutions develop, it is natural to look for a relevant solution in the Taylor series form

$$a_i=\frac{1}{\sqrt{k}}[a_{i,3}(x\sqrt{k})^3+a_{i,5}(x\sqrt{k})^5+\ldots]=a_{i,3}kx^3+a_{i,5}k^2x^5+\ldots, \quad i\geq 2. \tag{19}$$

and consider only a limited number of terms. The larger is this number, the larger is the accuracy of the solution. Note that eq. (10) also contains polynomial terms, but in that case Taylor series solutions would require infinite terms because the solution is needed over the whole time line, thus being practically useless. Note also that a solution in the form (19) resembles the classical machinery of center manifold theory [11].

The nonlinearity parameter k has been explicitly singled out so that the Taylor coefficients $a_{i,l}$ are functions of the axial parameter Γ only. The constant terms $a_{i,0}$ vanish because the manifold passes through the saddle point $x=a_i=0$. The linear terms $a_{i,1}$ are equal to zero because the manifold is tangent to the linear manifold (which is described by $a_i=0$, $i\geq 2$) at the saddle. Even powers $a_{i,2n}$ are not present because eq. (1) is symmetric, i.e., both $w(z,t)$ and $-w(z,t)$ are solutions.

To determine the remaining unknown numbers $a_{i,l}$, we insert (19) in (18) and expand in Taylor series. Accounting for (9) we obtain recursive sets of *linear* algebraic equations yielding the solution.

Equating the coefficients of x^3 to zero we get

$$a_{i,3}=\frac{d_{1,1}d_{1,i}}{9\Lambda_1-\Lambda_i},\qquad i\geq 2, \tag{20}$$

from which we see that the no internal resonance conditions $9\Lambda_1\neq\Lambda_i$, $i\geq 2$ must be satisfied to avoid singularities due to interactions between modes. Note that these relations certainly hold if $\Lambda_1<\Lambda_i$, $i\geq 2$, as it always occurs, e.g., in the range $\Gamma\in]\Gamma_{cr,1};\Gamma_{cr,2}[$ (Fig. 3).

Equating the coefficients of x^5 to zero we get

$$a_{i,5}=\frac{1}{25\Lambda_1-\Lambda_i}\left\{-6d_{1,1}^2a_{i,3}+\sum_{n=2}^{\infty}a_{n,3}(d_{1,1}d_{i,n}+2d_{1,i}d_{1,n})\right\},\qquad i\geq 2, \tag{21}$$

where $a_{i,3}$ are given by (20). Equation (21) adds the no internal resonance conditions $25\Lambda_1\neq\Lambda_i$, $i\geq 2$, which again are certainly satisfied if $\Lambda_1<\Lambda_i$, $i\geq 2$.

Obtaining higher order terms is much more difficult, and the coefficients $a_{i,l}$, $l=7,9,\ldots$, have very involved expressions. We do not pursue the relevant computations, but only infer from (20) and (21) that further no internal resonance conditions $l^2\Lambda_1\neq\Lambda_i$, $i\geq 2$, are to be satisfied, which certainly occurs if $\Lambda_1<\Lambda_i$, $i\geq 2$.

For the *first* family of b.c. we have $d_{1,i}=0$, $i\geq 2$, so that, from (20), $a_{i,3}=0$ and then, from (21), $a_{i,5}=0$. It is easy to infer that in this case $a_{i,l}=0$, $i\geq 2$, $\forall l$. This confirms that the nonlinear invariant manifold coincides with the linear one, namely, it is planar. This case corresponds to what Rosenberg [10] called *similar normal modes*, which are solutions of (18) in the linear form $a_i(x)=c_ix+e_i$, and practically entails solving

$$c_i\frac{\partial V}{\partial x}=\frac{\partial V}{\partial a_i},\quad i\geq 2. \tag{22}$$

Actually, in the present case, being $c_i=e_i=0$, a special case of *vanishing* similar normal modes occurs. The previous points show a further property of the beam with the first family of b.c.: the relevant nonlinear dynamics at homoclinicity develop along similar normal modes, which in particular coincide with the linear normal modes.

For the *second* family of b.c. the coefficients $a_{i,3}$ and $a_{i,5}$ are not trivial. They are reported in Fig. 4, where four terms are considered in the sum for the computation of $a_{i,5}$ (see eq. (21)). First, we note that the maximum values of both $a_{i,3}$ and $a_{i,5}$ for the fixed-free case (Fig. 4c) are O(1), while in the remaining cases they are at least one order of magnitude smaller. From an engineering point of view, this fact and the cubical vanishing of Σ at $x=0$ mean that the non-flatness of the manifold, while theoretically important, has a minor practical relevance, apart from the fixed-free case. This holds in a wide range of Γ values, and confirms a preliminary observation in [30], which has shown

this property to hold for a fixed parameter value and for fixed-fixed b.c..

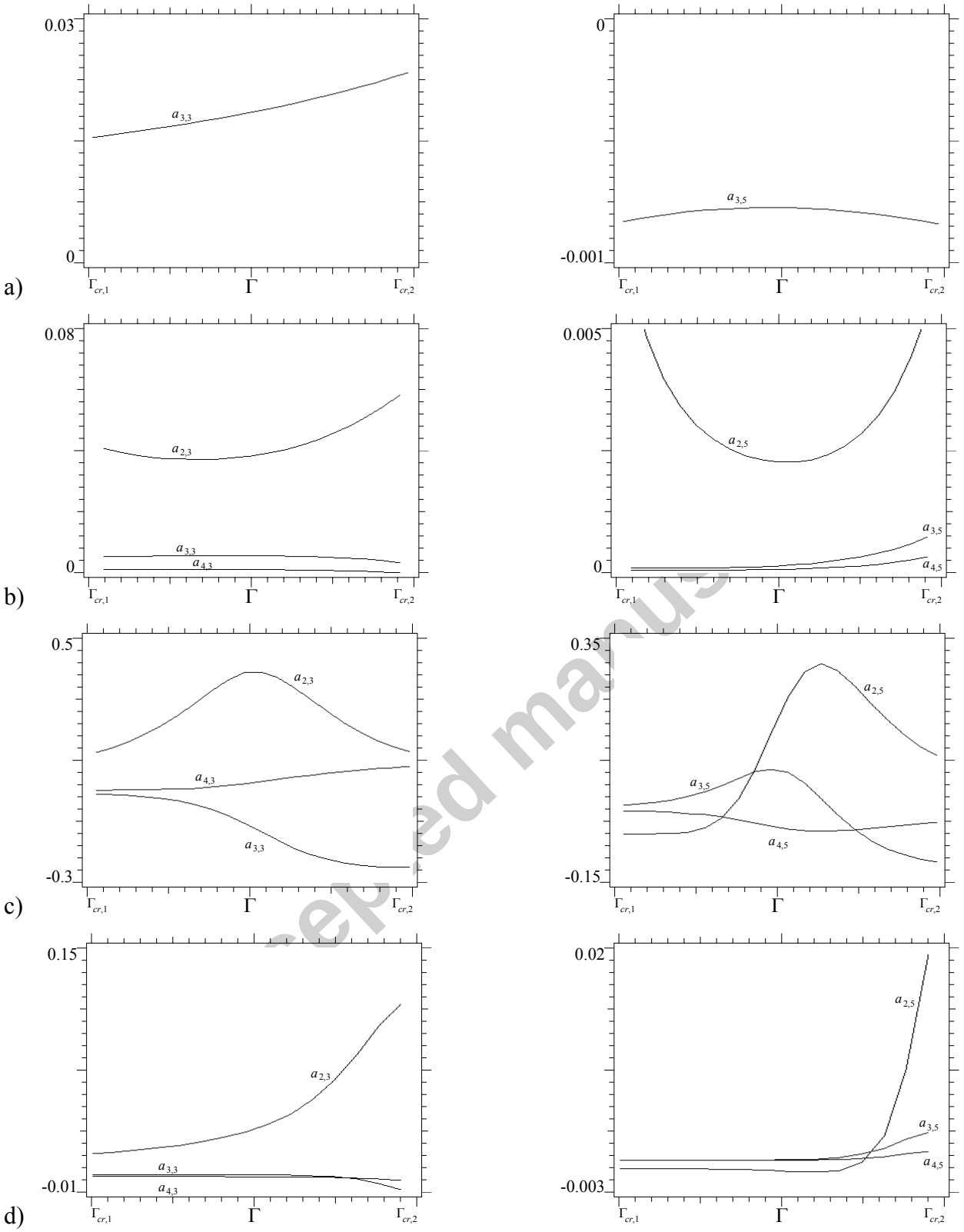

Figure 4. The first four coefficients $a_{i,3}$ and $a_{i,5}$ for a) fixed-fixed ($\Gamma_{cr,1}=4\pi^2$, $\Gamma_{cr,2}=8.1830\pi^2$; here $a_{2,3}=a_{4,3}=a_{2,5}=a_{4,5}=0$ because odd eigenfunctions satisfy $w_{2n-1}(1/2+z)=w_{2n-1}(1/2-z)$ while even eigenfunctions satisfy $w_{2n}(1/2+z)=-w_{2n}(1/2-z)$, so that $d_{n,m}=0$ if n is odd and m is even), b) fixed-hinged ($\Gamma_{cr,1}=2.0457\pi^2$, $\Gamma_{cr,2}= 6.0468\pi^2$), c) fixed-free ($\Gamma_{cr,1}=\pi^2/4$, $\Gamma_{cr,2}=9\pi^2/4$) and d) fixed-guided ($\Gamma_{cr,1}=\pi^2$, $\Gamma_{cr,2}=4\pi^2$) beams. The coefficients $a_{i,5}$ are computed with 4 terms in the sum in (21).

The second observation following from Fig. 4 is that, on average, $a_{i,5}$ is one order of magnitude smaller than $a_{i,3}$, showing how the *higher order nonlinearities* (Taylor coefficients $a_{i,l}$) in the slave modal amplitudes are important only for some isolated cases. Furthermore, still on average, both $a_{i,3}$ and $a_{i,5}$ are decreasing functions of i in absolute value. This means that *high order slave amplitudes* are practically unessential. A remarkable exception is, again, the fixed-free b.c. (Fig. 4c).

Finally, we note that $a_{i,3}$ and $a_{i,5}$ can have different signs for fixed values of Γ, showing how the non-flat manifold Σ can have complicated shapes in phase space.

Another simplification occurs for symmetric b.c., as the fixed-fixed ones of Fig. 2a. In this case, the odd eigenfunctions are symmetric with respect to the point z=1/2, namely, $w_{2n-1}(1/2+z) = w_{2n-1}(1/2-z)$, while the even eigenfunctions are anti-symmetric, $w_{2n}(1/2+z)=-w_{2n}(1/2-z)$, so that they are mutually orthogonal and $d_{n,m}=0$ if n is odd and m even (or viceversa). In other words, odd and even eigenfunctions span two orthogonal subspaces.

5. Reduced order models (ROMs)

By inserting the $a_i(x)$ obtained in the previous section in the expression $(9)_2$ of the potential $V(x,a_i(x))$ we get, after some computations,

$$V(x)=\frac{1}{2k}\{\alpha_2(x\sqrt{k})^2+\alpha_4(x\sqrt{k})^4+\alpha_6(x\sqrt{k})^6+\alpha_8(x\sqrt{k})^8+\ldots\}=\frac{1}{2}\{\alpha_2x^2+\alpha_4kx^4+\alpha_6k^2x^6+\alpha_8k^3x^8+\ldots\},$$

$$\alpha_2=\Lambda_1<0, \qquad \alpha_4=\frac{d_{1,1}^2}{2}>0, \qquad \alpha_6=\sum_{n=2}^{\infty}[\Lambda_n(a_n^3)^2+2d_{1,1}d_{1,n}a_n^3]=d_{1,1}^2\sum_{n=2}^{\infty}d_{1,n}^2\frac{18\Lambda_1-\Lambda_n}{(9\Lambda_1-\Lambda_n)^2},$$

$$\alpha_8=\sum_{n=2}^{\infty}[(43\Lambda_1-\Lambda_n)a_{n,3}a_{n,5}+6d_{1,1}^2(a_{n,3})^2], \tag{23}$$

where again the parameter k has been singled out, and where $a_{n,3}$ and $a_{n,5}$ are given by (20) and (21).

In what follows we assume that $\Gamma\in]\Gamma_{cr,1};\Gamma_{cr,2}[$, which is the region of main practical interest. This implies that $\Lambda_1<0$ and $\Lambda_n>0$, $n\geq2$, and thus easily proves that α_6 is negative. The sign of α_8, on the other hand, is not known in advance (see Fig. 5 below).

The coefficients α_i are at the base of the reduced order models (single d.o.f., indeed) obtained in this section, and α_i, i=6,8,…, summarize the effects of non-flatness of the manifold Σ. They are

$$\alpha_2=\pi^2(\pi^2-\Gamma), \qquad \alpha_4=\frac{\pi^4}{2}, \qquad \alpha_i=0,\ i=6,8,\ldots, \qquad \text{(hinged-hinged beam)},$$

$$\alpha_2=(\pi/2)^2[(\pi/2)^2-\Gamma], \qquad \alpha_4=\frac{\pi^4}{32}, \qquad \alpha_i=0,\ i=6,8,\ldots, \qquad \text{(guided-hinged beam)}, \tag{24}$$

for the first family of b.c. (of course α_i=0, i=6,8,…, because in this case the manifold is flat), while they are reported in Fig. 5 for the second family of b.c.. Four slave amplitudes are used in the summations of (23). This appears sufficient apart from the singular trend of α_8 close to $\Gamma_{cr,2}$ for fixed-hinged (Fig. 5b) and fixed-guided (Fig. 5d) b.c., where more terms are likely required.

a) fixed-fixed ($\Gamma_{cr,1}=4\pi^2$, $\Gamma_{cr,2}=8.1830\pi^2$)

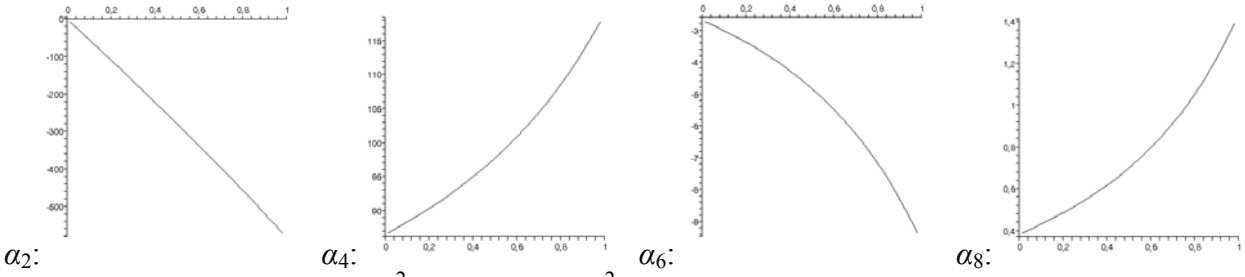

α_2: α_4: α_6: α_8:

b) fixed-hinged ($\Gamma_{cr,1}=2.0457\pi^2$, $\Gamma_{cr,2}= 6.0468\pi^2$)

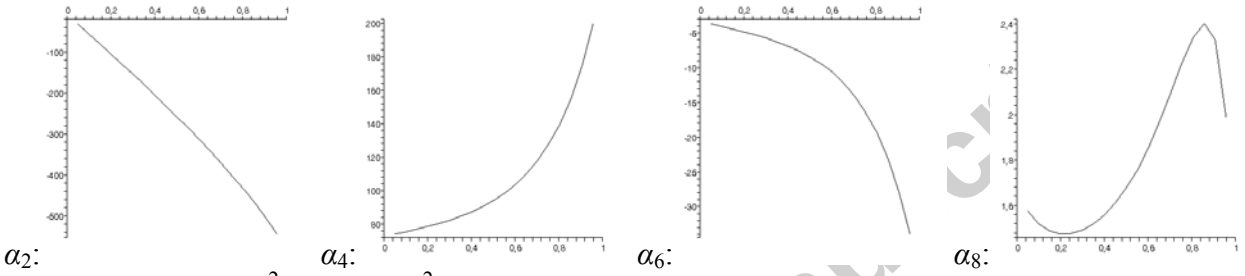

α_2: α_4: α_6: α_8:

c) fixed-free ($\Gamma_{cr,1}=\pi^2/4$, $\Gamma_{cr,2}=9\pi^2/4$)

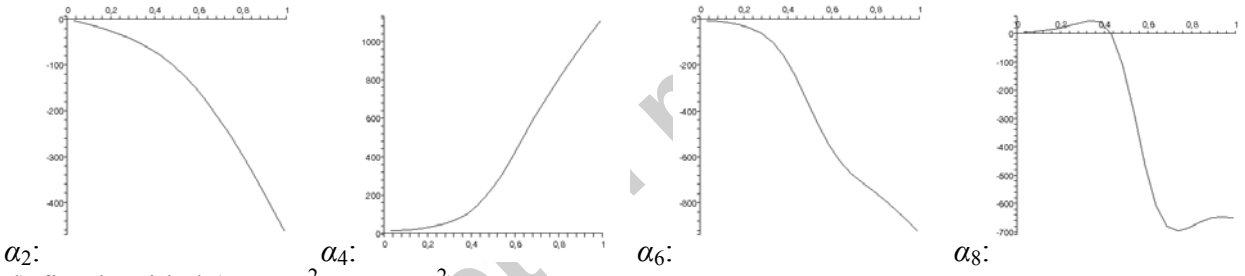

α_2: α_4: α_6: α_8:

d) fixed-guided ($\Gamma_{cr,1}=\pi^2$, $\Gamma_{cr,2}=4\pi^2$)

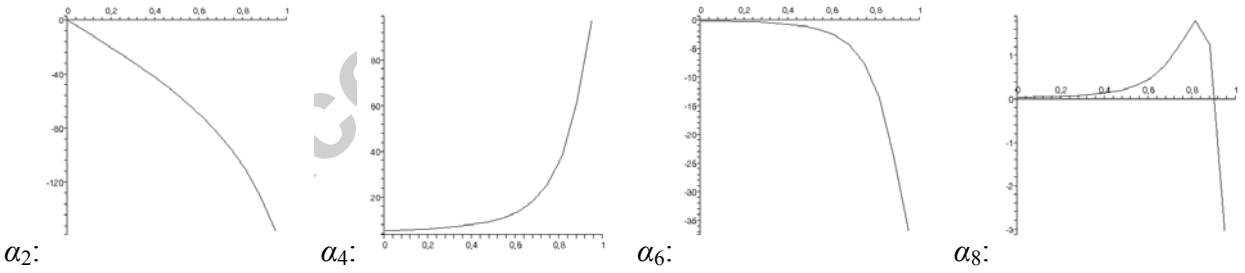

α_2: α_4: α_6: α_8:

Figure 5. The coefficients α_2, α_4, α_6 and α_8 for the second family of b.c.. The coefficients α_6 and α_8 are computed with 4 terms in the sums in (23). The abscissa ranges from $\Gamma_{cr,1}$ to $\Gamma_{cr,2}$.

The equation of motion is

$$\ddot{x}+\frac{dV}{dx}=\ddot{x}+\alpha_2 x+2\alpha_4 k x^3+3\alpha_6 k^2 x^5+4\alpha_8 k^3 x^7+\ldots=0, \tag{25}$$

while the homoclinic orbit of the hilltop saddle, whose determination is the main object of this work, can be obtained by solving

$$\frac{dx}{dt}=\sqrt{-2V(x)}=\sqrt{-\alpha_2 x^2-\alpha_4 k x^4-\alpha_6 k^2 x^6-\alpha_8 k^2 x^8-\dots}\,. \tag{26}$$

It is useful to perform the following change of variables

$$y=\left(\frac{\alpha_4 k}{-\alpha_2}\right)x^2, \qquad \tau=2t\sqrt{-\alpha_2}\,, \tag{27}$$

so that (26) becomes

$$\frac{dy}{d\tau}=y\sqrt{1-y+\beta_2 y^2-\beta_3 y^3+\dots}\,, \qquad \beta_2=\frac{\alpha_2\alpha_6}{(\alpha_4)^2}, \qquad \beta_3=\frac{\alpha_2^2\alpha_8}{(\alpha_4)^3}, \dots. \tag{28}$$

which is k-independent. Note also that with this change of variables the two symmetric homoclinic loops coincide, so that in terms of y we have only one homoclinic solution.

Integrating (28) we obtain the expression $\tau=\tau(y)$ of the homoclinic loop

$$\tau=-\int_{y}^{\bar{y}}\frac{d\xi}{\xi\sqrt{1-\xi+\beta_2\xi^2-\beta_3\xi^3+\dots}}, \tag{29}$$

where $\bar{y}=y_{\mathrm{hom}}(0)$ is the smallest positive solution of $1-y+\beta_2 y^2-\beta_3 y^3+\dots=0$. It represents the maximum extension of the homoclinic loop, which in fact belongs to the interval $y\in[0,\bar{y}]$. Finally, $y_{\mathrm{hom}}(\tau)$ can be obtained by inverting (29).

Equations (23) and (25) provide a *hierarchy* of approximate reduced order, single d.o.f., models (ROMs), obtained by accounting for an increasing number l of higher order nonlinearities $a_{i,l}$ in the ith slave amplitude.

5.1. Unrefined ROM

If we neglect α_6, α_8,…, i.e., consider a quartic potential, we obtain

$$\ddot{x}+\alpha_2 x+2\alpha_4 k x^3=0, \tag{30}$$

which is the well-known Duffing equation. It corresponds to the governing equation obtained by the classical (linear) Galerkin projection of the dynamics onto the first linear mode. In fact, it is easy to verify that if we assume $w(z,t)=x(t)w_1(z)$, insert this expression in (1), multiply by $w_1(z)$ and integrate from $z=0$ to $z=1$, we get (30). It is worth to remark that (30) provides an *exact* result for the first family of b.c., for which $\alpha_i=0$, $i=6,8,\dots$, whereas just an unrefined *approximation* for the second family. In the latter case, it can be considered as a *minimal* approximation, in the sense that

it is the simplest ROM permitting to approximate the homoclinic orbits of interest.

The homoclinic loop of eq. (30) can be computed in closed form, by integrating and then inverting (29). This yields

$$y_{3,\mathrm{hom}}(\tau)=\frac{2}{1+\cosh(\tau)}, \tag{31}$$

which, in these variables, is independent of k and Γ, namely of the b.c..

5.2. First refined ROM

For the second family of b.c. it is possible to improve the approximation by considering α_6 and neglecting higher order terms. The equation of motion becomes

$$\ddot{x}+\alpha_2 x+2\alpha_4 k x^3+3\alpha_6 k^2 x^5=0. \tag{32}$$

To proceed with the computation of the homoclinic solution, we need $\bar{y}$, which at the considered order is given by

$$\bar{y}=\frac{1-\sqrt{1-4\beta_2}}{2\beta_2}. \tag{33}$$

We see that $\bar{y}$ exists if and only if $\beta_2<1/4$. This suggests that this model must be considered with care. In fact, from (23) we know that α_6 is always negative, see Fig. 5 (and then β_2 is positive), so that, strictly speaking, this approximation corresponds to a softening oscillator, which is in contrast with the original mechanical system, which is certainly hardening.

However, for α_6 sufficiently small (and thus for β_2 small), the softening "error" manifests itself for only large values of y, and far from the region of practical interest, which is that occupied by the homoclinic loop (see Fig. 12a below). In this case, $\bar{y}$ and the homoclinic solution certainly exist.

When $|\alpha_6|$ (and β_2) increase, the escape region approaches the homoclinic orbit, and the approximation (32) is initially no longer reliable, and then fails to possess a homoclinic orbit (when point B in Fig. 12a collapses onto point A on the zero potential line). This occurs when $\beta_2=1/4$. To illustrate how this threshold depends on the b.c., we have reported in Fig. 6 the parameter $\beta=\sqrt{1-4\beta_2}$ appearing in (33), which is central for this model (note that $\beta=1$ corresponds to the unrefined ROM). It is always imaginary for the case of fixed-free b.c., which again shows a different behaviour with respect to the other b.c. of the second family.

Above the thresholds $\beta=0$ highlighted in Fig. 6, the ROM (32) is meaningless, and one must retain higher order terms. To reproduce the hardening behaviour at infinity, one must have a positive highest order coefficient of the considered approximation. In several cases, but not always,

this can be obtained by considering terms up to α_8 (see Fig. 5).

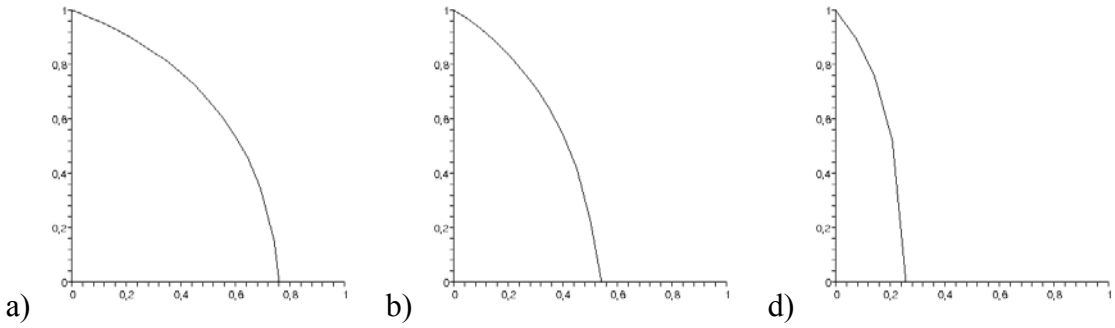

Figure 6. The parameter $\beta=\sqrt{1-4\beta_2}$ for a) fixed-fixed ($\Gamma_{cr,1}=4\pi^2$, $\Gamma_{cr,2}=8.1830\pi^2$), b) fixed-hinged ($\Gamma_{cr,1}=2.0457\pi^2$, $\Gamma_{cr,2}=6.0468\pi^2$) and d) fixed-guided ($\Gamma_{cr,1}=\pi^2$, $\Gamma_{cr,2}=4\pi^2$) beams. The abscissa ranges from $\Gamma_{cr,1}$ to $\Gamma_{cr,2}$.

Below the threshold, on the other hand, the present approximation can be practically used, although with a varying degree of reliability. The homoclinic loop of the saddle $x=0$ can again be computed in closed form, by integrating and then inverting (29):

$$y_{5,\mathrm{hom}}(\tau)=\frac{2}{1+\beta\cosh(\tau)}. \tag{34}$$

The possibility to have an analytical expression for the homoclinic orbit makes model (32) interesting in any case. By comparing (34) with (31) we can appreciate the effects of the non-planarity of the manifold (up to its lowest order) on the homoclinic loop. Fig. 7 reports the time histories and the phase portraits, holding for all b.c., from which we note a marked difference, even for β not so far from 1, i.e., even for Γ not so larger than $\Gamma_{cr,1}$ (Fig. 6).

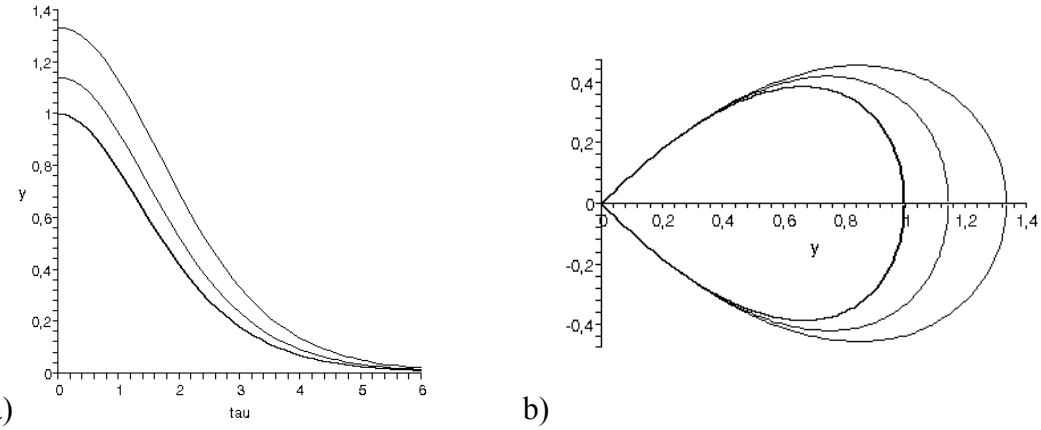

Figure 7. Homoclinic loops $y_{3,\mathrm{hom}}(\tau)$ (thick line, $\beta=1$) and $y_{5,\mathrm{hom}}(\tau)$ (thin lines, $\beta=0.75$ and $\beta=0.5$). a) time histories and b) phase portraits.

A more synthetic comparison is provided by the ratio

$$\delta(\tau)=\frac{y_{5,\mathrm{hom}}(\tau)}{y_{3,\mathrm{hom}}(\tau)}=\frac{1+\cosh(\tau)}{1+\beta\cosh(\tau)}, \tag{35}$$

which ranges from $\delta(0)=2/(1+\beta)$ to $\delta(\infty)=1/\beta$ and is depicted in Fig. 8. The differences are important from an engineering point of view, showing that the non-planarity of Σ cannot be neglected, even for practical purposes. Note that the asymptotically attained difference is greater than the initial one.

To better visualize the effects of the non-planarity, we have drawn in a 3D section of the phase space (Fig. 9) the invariant manifold Σ with the homoclinic loop $y_{5,\mathrm{hom}}(\tau)$, its projection on the plane $(y, \dot{y})$, and its approximation $y_{3,\mathrm{hom}}(\tau)$, which, as said, is obtained by the classical Galerkin projection of the original infinite dimensional system onto the first mode. Note that the vertical direction is blown-up to highlight the non-flatness of the manifold.

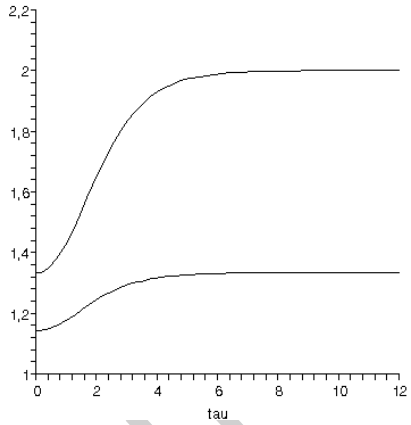

Figure 8. The ratio $\delta(\tau)$ for β=0.75 (lower curve) and β=0.5 (upper curve).

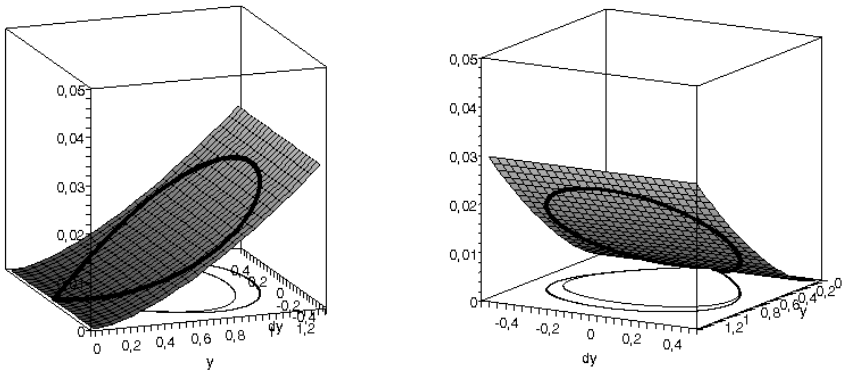

Figure 9. The invariant manifold Σ, the homoclinic loop $y_{5,\mathrm{hom}}(\tau)$ (very thick line), its projection on the plane $(y, \dot{y})$ (thick line) and its approximation $y_{3,\mathrm{hom}}(\tau)$ (thin line) in the space $(y, \dot{y}, a_2)$.

β=0.75 and $\gamma=\frac{b_2^3}{\sqrt{k}}\left(\frac{-\alpha_2}{\alpha_4}\right)^{3/2}$=0.02, being $a_2=a_{2,3}\,kx^3=\gamma y^{3/2}$.

5.3. Second refined ROM

A more refined model is obtained by considering terms up to α_8 in (25), which becomes

$$\ddot{x}+\alpha_2 x+2\alpha_4 k x^3+3\alpha_6 k^2 x^5+4\alpha_8 k^3 x^7=0. \tag{36}$$

This model reproduces the hardening behaviour of the original system if $\alpha_8>0$, which is therefore assumed in the following (Fig. 5).

To determine $\bar{y}$ we have to solve $0=1-y+\beta_2 y^2-\beta_3 y^3$. Depending on the values of β_2 and β_3, this equation can have one or three real solutions. The regions of different behaviour are depicted in white and gray in Fig. 10, respectively. The former case corresponds to a two-well potential, while the latter corresponds to a four-well potential (Fig. 10), a situation which is not expected in practice. In fact, it is also shown in Fig. 10 that the actual curve $(\beta_2(\Gamma),\beta_3(\Gamma))$ for the fixed-fixed b.c. does not cross the grey area, so that, as expected, in the real case there is only one solution $\bar{y}$, which is depicted in Fig. 11 as a function of Γ. When compared with $\bar{y}(\Gamma)=1$ of the unrefined ROM (see Sect. 5.1), this figure shows again that the non-flatness of the manifold Σ may have non-negligible effects. Figure 11 (as well as Fig. 7b) shows that the linear Galerkin method produces the maximum underestimation of $\bar{y}$, which corresponds to the stiffest approximation of the real system ensuing from projection of its global dynamics onto the first mode (master amplitude) with no contributions from the higher order modes (slave amplitudes).

Similar situations occur with the other b.c. of the second family, at least for Γ far away from $\Gamma_{cr,2}$, which are not reported to limit the length of the paper.

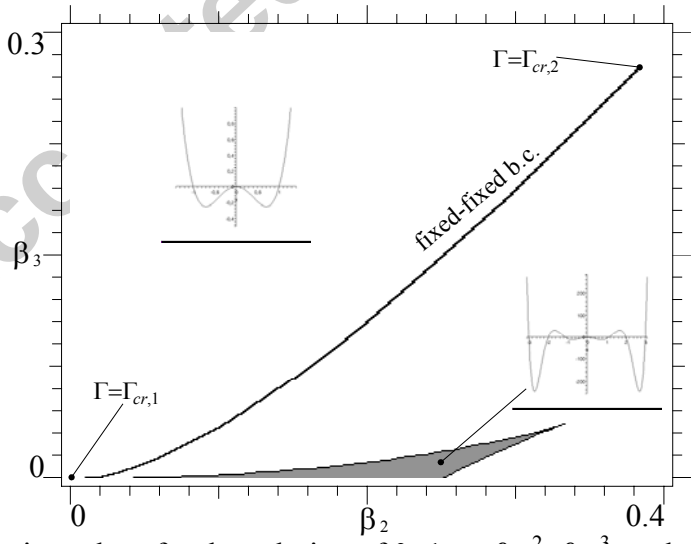

Figure 10. Behaviour chart for the solution of $0=1-y+\beta_2 y^2-\beta_3 y^3$, and parametric curve $(\beta_2(\Gamma),\beta_3(\Gamma))$ for fixed-fixed b.c.

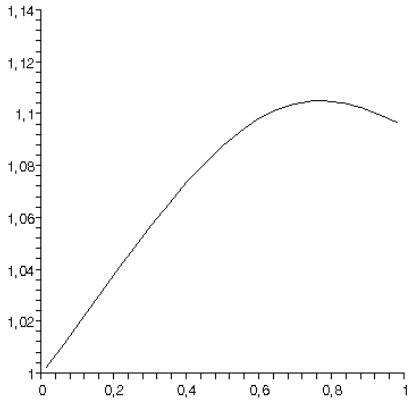

Figure 11. The curve $\bar{y}(\Gamma)$ for fixed-fixed b.c. and for $\Gamma \in [\Gamma_{cr,1}, \Gamma_{cr,2}]$.

Once $\bar{y}$ is known, we can compute the integral (29) in closed form (although with a complex formula), but unfortunately we are not able to invert the expression $\tau=\tau(y)$; thus we have no analytical expression of $y_{7,\mathrm{hom}}(\tau)$, although it can be easily obtained numerically. However, the effects of the manifold curvature on the homoclinic solution evidenced in Fig. 11 are sufficient to remark its importance, so that we do not pursue the computation of $\tau=\tau(y)$ further on.

5.4. Comparisons between ROMs

In this section we compare the results obtained with the three ROMs previously introduced. We consider only the fixed-fixed case. Furthermore, as we want to perform a comparison of the physical potentials $V(x)$, we use the true master amplitude x instead of its abstract version y, however accounting for the relevant symmetry.

The potentials $V_4(x)$, $V_6(x)$ and $V_8(x)$ of the three ROMs are reported in Fig. 12a, which shows the corrections due to the higher order nonlinearities. The corresponding phase portraits are reported in Fig. 12b. Apart from the quantitative differences, which are of the order of 10÷15%, we see that there is a non-monotonic convergence toward the limit potential V_∞ representing the exact homoclinic solution of the buckled beam.

The softening behaviour of the potential V_6 is clearly visible in Fig. 12a, because the considered value of Γ (corresponding to β=0.458) is not so far from the value $(\Gamma-\Gamma_{cr,1})/(\Gamma_{cr,2}-\Gamma_{cr,1})\cong 0.76$ corresponding to the critical threshold β=0 (see Fig. 6a). For smaller values of Γ, the right hilltop is higher and out of the chosen window; when Γ tends to $(\Gamma-\Gamma_{cr,1})/(\Gamma_{cr,2}-\Gamma_{cr,1})\cong 0.76$, on the other hand, point B collapses onto point A on the zero potential line.

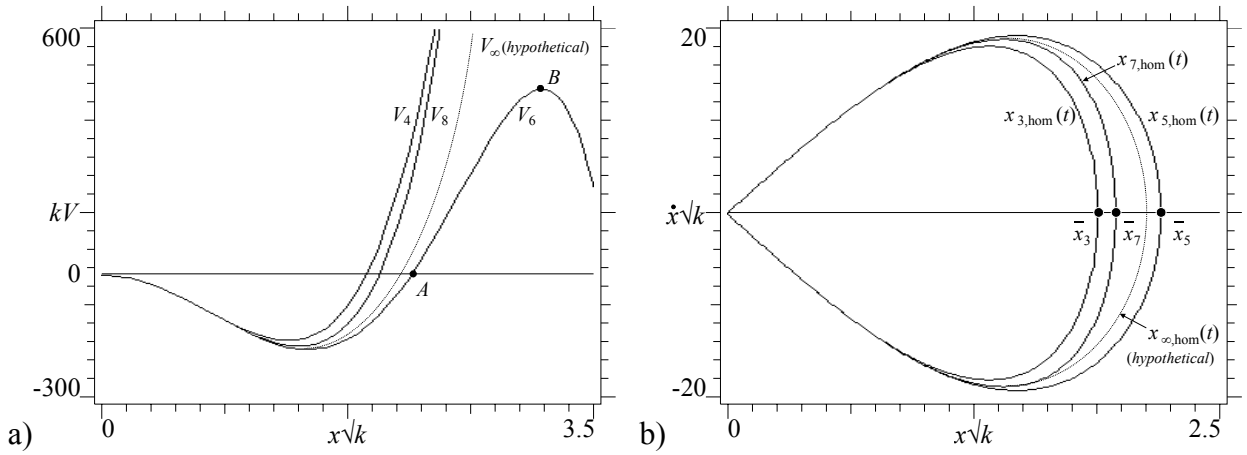

Figure 12. a) The potentials $kV_4(x\sqrt{k})$, $kV_6(x\sqrt{k})$ and $kV_8(x\sqrt{k})$ and b) the phase portrait of the homoclinic loops $x_{3,\mathrm{hom}}(t)$, $x_{5,\mathrm{hom}}(t)$ and $x_{7,\mathrm{hom}}(t)$. Fixed-fixed b.c., $(\Gamma-\Gamma_{cr,1})/(\Gamma_{cr,2}-\Gamma_{cr,1})\cong 0.64$.

To extend the previous comparison to other values of the axial parameter, we have depicted in Fig. 13 the maximum extension $\bar{x}$ of the homoclinic orbit as a function of Γ for the three models. Note that $\bar{x}_5$ exists only up to $(\Gamma-\Gamma_{cr,1})/(\Gamma_{cr,2}-\Gamma_{cr,1})\cong 0.76$ (see Fig. 6a), and in the neighborhood of this limit value the first refined ROM is not accurate. Figure 13 shows that just above the static buckling load $\Gamma_{cr,1}$ the effects of the non-planarity of the manifold Σ are negligible, while they become more and more important as the axial parameter increases.

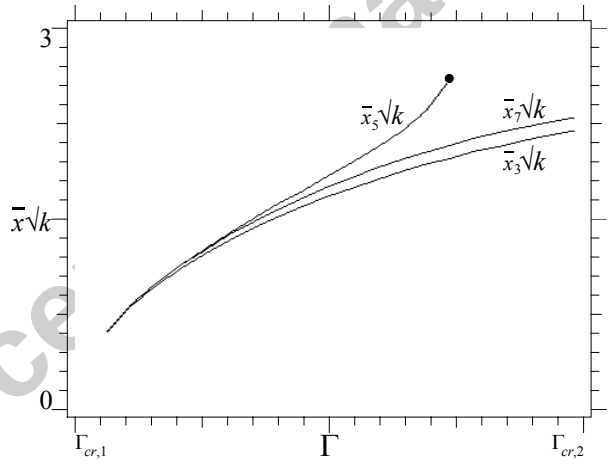

Figure 13. The maximum extension ($\bar{x}\sqrt{k}$) of the homoclinic orbit for the three ROMs. Fixed-fixed b.c..

The final comparison is made in terms of the analytical expressions of the homoclinic solution of the buckled beam, as provided by the three models:

$w_{\mathrm{hom}}(z,t)=x_{3,\mathrm{hom}}(t)w_1(z)$, unrefined ROM,

$w_{\mathrm{hom}}(z,t)=x_{5,\mathrm{hom}}(t)w_1(z)+\sum_{n=2}^{\infty} a_{n,3}k[x_{5,\mathrm{hom}}(t)]^3 w_n(z)$, first refined ROM,

$$w_{\mathrm{hom}}(z,t)=x_{7,\mathrm{hom}}(t)w_1(z)+\sum_{n=2}^{\infty}\{a_{n,3}k[x_{7,\mathrm{hom}}(t)]^3+a_{n,5}k^2[x_{7,\mathrm{hom}}(t)]^5\}w_n(z)\,,\quad \text{second refined ROM} \quad (37)$$

In the unrefined model (which is nonetheless exact for the first family of b.c.), the un-corrected master amplitude and time-independent spatial shape do occur. In contrast, in the refined models, the approximation of the master modal amplitude is improved by accounting for (a theoretically infinite number of) slave modal amplitudes $a_{n,l}$ at different l-orders. Of course, for practical purposes, the n-summations in (37) can be limited to only few terms. Yet, irrespective of the considered number of terms, all of the refined models account, at different l-orders, for a twofold effect on the homoclinic orbit of the higher order modes described by the slave amplitudes. (i) They affect the solely time-dependent master *amplitude* of the first mode, which enters the homoclinic orbit expression at increasing power orders in the various refined models. (ii) They entail a *time varying spatial shape* of the homoclinic orbit ensuing from a nonlinear Galerkin projection of the solution onto the basis of linear normal modes. In both respects, apart from referring to homoclinic orbits and from being obtained based on *a priori* Galerkin projection of the dynamics in the spirit of the original (see the Introduction) NNM approach [12], the structure of the obtained solution closely resembles the refined structure of nonlinear displacement fields as provided *a posteriori* for a number of infinite-dimensional systems (see, e.g., [20]) by the alternative NNM approach [18, 19].

Finally, it would be worth: (i) To perform a convergence analysis aimed at evaluating the number of slave amplitudes to be considered for obtaining a reliable solution; (ii) to evaluate the relative importance of considering either one more higher-order nonlinearity within the chosen number of slave amplitude(s) or one more slave amplitude up to an overall lower-order level of nonlinearity; (iii) to compare the spatial shapes of the solution as provided by the various ROMs. All of these issues of main practical interest are left for possible future research.

6. Conclusions and further developments

The homoclinic solutions of an initially straight, planar buckled beam have been investigated in an infinite-dimensional context. Upon conjecturing that the homoclinic solutions exist and belong to a two-dimensional invariant manifold Σ, we have considered all possible boundary conditions and shown how they can be grouped in two families.

The *first* family includes the hinged-hinged and guided-hinged b.c.. Various relevant properties have been illustrated all along the paper. (i) An *exact* solution of the system PDE can be pursued in the form of separate variables; (ii) the eigenvalues of the linearized PDE depend linearly on the governing parameter Γ representing the axial load; (iii) the associated projected (onto the linear normal modes) equations of motion have a very weak coupling; and (iv) the relevant nonlinear

dynamics at homoclinicity develop along similar normal modes (as defined by Rosenberg), which in particular coincide with the linear ones.

However, for the purposes of the present work, the most important properties are that (i) the invariant manifold Σ is *flat* (and coincides with the manifold spanned by the first eigenfunction), and that (ii) the homoclinic solutions can be easily calculated in analytical form. They coincide with those computed via the (linear) Galerkin projection onto the solely first mode.

These properties are *no longer* valid for the *second* family, which contains all of the remaining b.c.. In particular, no exact expressions of the homoclinic solutions are directly found for these b.c., so that we have attacked the problem by means of the NNM technique [10]. This provides series expressions of the manifold Σ and of the homoclinic orbits, and requires to solve an infinite sequence of linear algebraic problems. Only few terms are indeed sufficient for practical purposes, so that only approximate manifolds and orbits are considered.

As a matter of fact, there are two kinds of approximations. The first is concerned with the *number* of *linear normal modes* used to span the space of admissible functions. The second with the *order* of the *highest nonlinear term* considered in the Taylor expansion of the functions describing the *non-planar* manifold. As to the former, we have identified the amplitude of the first linear eigenfunction as the solely independent variable, with all of the other modes being considered as dependent variables. Thus, we have considered single d.o.f. models. As to the latter, we have obtained a hierarchy of *reduced order models* based on successive approximations of the potential. The simplest one, corresponding to a quartic potential, is the classical Duffing oscillator obtained by the linear Galerkin projection. A first refined model is obtained by considering up to the sixth term in the potential, a second refined model up to the eighth term, and so on. The first three ROMs have been analyzed in detail and compared with each other.

It has been shown that, while being always important from a theoretical point of view, the non-planarity of the manifold where the homoclinic solutions lie becomes increasingly important also from a practical point of view when the axial parameter grows much above the buckling value.

The analysis in this paper is a necessary step in the involved process of detecting chaotic dynamics in infinite dimensional systems. The next step consists of evaluating how damping and excitation modify the homoclinic orbits. Indeed, it is known that, depending on the relative amplitudes of these parameters, homoclinic orbits may survive or disappear, and that the boundary between the two different regimes is given by the homoclinic bifurcation. This global event can be detected by means of the Holmes and Marsden [31] theorem, which is an infinite-dimensional extension of the classical Melnikov method [5]. For fixed-fixed b.c. and for a given value of Γ close to $\Gamma_{cr,1}$, this has been done in [30]. The results of the present work strongly call for a generalization

of the homoclinic bifurcation analysis to other values of the axial parameter and to different b.c.

References

[1] C. Grebogi, E. Ott, J.A. Yorke, Crises, Sudden Changes in Chaotic Attractors, and Transient Chaos, Physica D 7 (1983) 181-200.

[2] F.C. Moon, J. Cusumano, P. Holmes, Evidence for Homoclinic Orbits as a Precursor to Chaos in a Magnetic Pendulum, Physica D 24 (1987) 383-390.

[3] A.L. Katz, E.H. Dowell, From Single Well Chaos to Cross Well Chaos: A Detailed Explanation in Terms of Manifold Intersections, Int. J. Bifur. Chaos, 4 (1994) 933-941.

[4] J.M.T. Thompson, G.H.M. van der Heijden, Homoclinic orbits, spatial chaos and localized buckling, IUTAM Symposium on 'New Applications of Nonlinear and Chaotic Dynamics in Mechanics', Cornell, 1997 (ed. F.C. Moon, Kluwer, Dordrecht, 1999, pp. 127-138).

[5] J. Guckenheimer, P. Holmes, Nonlinear Oscillations, Dynamical Systems and Bifurcation of Vector Fields, Springer-Verlag, New York, 1983.

[6] D. Hobson, An Efficient Method for Computing Invariant Manifolds of Planar Maps, J. Comput. Physics 104 (1993) 14-22.

[7] I. Blekhman, Vibrational Mechanics, World Scientific, Singapore-London-Hong Kong, 2000.

[8] A. Steindl, H. Troger, Methods for dimension reduction and their application in nonlinear dynamics, Int. J. Solids Struct. 38 (2001) 2131-2147.

[9] G. Rega, H. Troger (eds.), Dimension Reduction of Dynamical Systems: Methods, Models, Applications, Special Issue of Nonlin. Dyn. 41 (2005).

[10] R.H. Rand, Lecture Notes on Nonlinear Vibrations, Cornell University, available on line at www.tam.cornell.edu/randdocs/, 2003.

[11] H. Troger, A. Steindl, Nonlinear Stability and Bifurcation Theory, Springer-Verlag, Wien, 1991.

[12] R.M. Rosenberg, The normal modes of nonlinear n-degrees-of-freedom systems, ASME J. Appl. Mech. 30 (1962) 7-14.

[13] R.H. Rand, A direct method for non-linear normal modes, Int. J. Non-Lin. Mech. 9 (1974) 363-368.

[14] A.F. Vakakis, Analysis and identification of linear and nonlinear normal modes in vibrating systems, Ph.D. Dissertation, California Institute of Technology, Pasadena, CA, 1990.

[15] S.W. Shaw, C. Pierre, Non-linear normal modes and invariant manifolds, J. Sound Vibr. 150 (1991) 170-173.

[16] S.W. Shaw, C. Pierre, Normal modes for nonlinear vibratory systems, J. Sound Vibr. 164 (1993) 85-124.

[17] W.C. Xie, H.P. Lee, S.P. Lim, Normal modes of a non-linear campled-clamped beam, J. Sound Vibr. 250 (2002) 339-349.

[18] C. Pak, R.H. Rand, F.C. Moon, Free vibrations of a thin elastica by normal modes, Nonlin. Dyn. 3 (1992) 347-364.

[19] A.H. Nayfeh, On direct methods for constructing nonlinear normal modes of continuous systems, J. Vibr. Control 1 (1995) 389-430.

[20] W. Lacarbonara, G. Rega, A.H. Nayfeh, Resonant nonlinear normal modes. Part I: Analytical treatment for one-dimensional structural systems, Int. J. Non-Lin. Mech. 38 (2002) 851-872.

[21] N. Srinil, G. Rega, Two-to-one resonant multi-modal dynamics of horizontal/inclined cables. Part II: Internal resonance activation, reduced order models and nonlinear normal modes, Nonlin. Dyn. to appear (2006).

[22] C.E.N. Mazzilli, M.E.S. Soares, G.P. Baracho Neto, Non-linear normal modes of a simply supported beam: continuos system and finite-element models, Comp. Struct. 82 (2004) 2683-2691.

[23] E. Pesheck, C. Pierre, S. Shaw, Accurate reduced-order models for a simple rotor blade model using nonlinear normal modes, Mathematical and Computer Modelling 33 (2001) 1085-1097.

[24] W.C. Xie, H.P. Lee, S.P. Lim, Nonlinear dynamic analysis of MEMS switches by nonlinear modal analysis, Nonlin. Dyn. 31 (2003) 243-256.

[25] E. Mettler, Dynamic Buckling, Chap. 62 of Handbook of Engineering Mechanics, W. Flügge (Ed.), McGraw-Hill, New York, 1962.

[26] P. Villaggio, Mathematical Models for Elastic Structures, Cambridge University Press, Pisa, 1997.

[27] H. Kauderer, Nichtlineare Mechanik, Springer, Berlin, 1958.

[28] A.F. Vakakis, L.I. Manevitch, Y.V. Mikhlin, V.N. Pilipchuck, A.A. Zevin, Normal Modes and Localization in Nonlinear Systems, Wiley, 1996.

[29] A.H. Nayfeh, Nonlinear Interactions, Wiley Interscience, New York, 2000.

[30] S. Lenci, G. Rega, Optimal control of the homoclinic bifurcation in buckled beams: infinite-dimensional vs reduced order modeling, in Recent Advances in Nonlinear Mechanics (RANM2005), 30 August - 1 September 2005, Aberdeen, Scotland, UK.

[31] P. Holmes, J. Marsden, A Partial Differential Equation with Infinitely many Periodic Orbits: Chaotic Oscillations of a Forced Beam, Arch. Rat. Mech. Anal. 76 (1981) 135-165.

[32] Y.C. Fung, A. Kaplan, Buckling of Low Arches or Curved Beams of Small Curvature, U.S. National Advisory Committee for Aeronautics, Technical Note 2840 (1952).